HHS Public Access

Author manuscript

*ACS Energy Lett*. Author manuscript; available in PMC 2018 November 30.

Published in final edited form as:

*ACS Energy Lett*. 2018 July 13; 3(7): 1571–1577. doi:10.1021/acsenergylett.8b00835.

# Spontaneous Silver Doping and Surface Passivation of $CsPbI_3$ Perovskite Active Layer Enable Light-Emitting Devices with an External Quantum Efficiency of 11.2%

**Min Lu**[#†], **Xiaoyu Zhang**[#†,‡], **Xue Bai**[*,†], **Hua Wu**[†], **Xinyu Shen**[†], **Yu Zhang**[*,†], **Wei Zhang**[‡], **Weitao Zheng**[‡], **Hongwei Song**[†], **William W. Yu**[†,§], and **Andrey L. Rogach**[*,‖]

[†]State Key Laboratory of Integrated Optoelectronics and College of Electronic Science and Engineering, Jilin University, Changchun 130012, China

[‡]Department of Materials Science, Key Laboratory of Mobile Materials MOE, State Key Laboratory of Automotive Simulation and Control, Jilin University, Changchun 130012, China

[§]Department of Chemistry and Physics, Louisiana State University, Shreveport, Louisiana 71115, United States

[‖]Department of Materials Science and Engineering, and Centre for Functional Photonics (CFP), City University of Hong Kong, Kowloon, Hong Kong SAR

[#] These authors contributed equally to this work.

## Abstract

Lead halide perovskite nanocrystals are currently under intense investigation as components of solution-processed light-emitting devices (LEDs). We demonstrate LEDs based on Ag doped–passivated $CsPbI_3$ perovskite nanocrystals with external quantum efficiency of 11.2% and an improved stability. Ag and trilayer $MoO_3$/Au/$MoO_3$ structure were used as cathode and anode, respectively, which reduce the electron injection barrier and ensure the high transparency and low resistance of the anode. Silver ions diffuse into perovskite film from the Ag electrode, as confirmed by the elemental mapping, the presence of Ag 3d peaks in the X-ray photoelectron spectrum, and the peak shift in the X-ray diffraction patterns of $CsPbI_3$. In addition to doping, silver ions play the beneficial role of passivating surface defect states of $CsPbI_3$ nanocrystals, which results in increased photoluminescence quantum yield, elongated emission lifetime, and improved stability of perovskite films.

## Graphical Abstract

[*]**Corresponding Authors** baix@jlu.edu.cn. yuzhang@jlu.edu.cn. andrey.rogach@cityu.edu.hk.

ASSOCIATED CONTENT

Supporting Information

The Supporting Information is available free of charge on the ACS Publications website at DOI: 10.1021/acsenergylett.8b00835. Experimental details on materials synthesis, device fabrication, and characterizations; EQEs for 26 Agdoped $CsPbI_3$ NC-based LEDs; Cs 3d XPS spectra; TEM images; elemental mapping; EDX spectrum; crosssectional SEM images; stability tests for Ag- and ITO-based devices; and optical spectra (PDF)

Notes

The authors declare no competing financial interest.

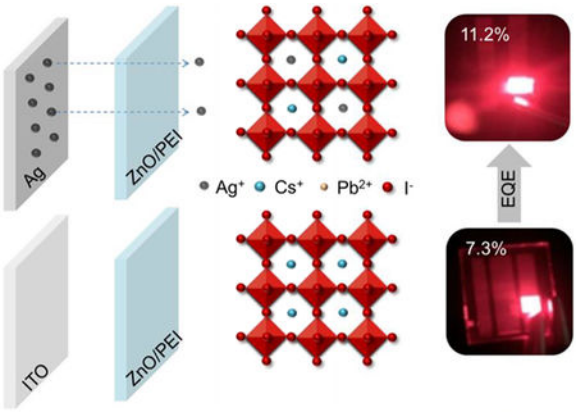


Lead halide perovskite nanocrystals (NCs) have attracted significant attention as components of solution-processed light-emitting devices (LEDs) because of their desirable optical characteristics such as high photoluminescence quantum yield (PL QY), narrow emission, and wide color range.[1–5] As a result of the rapid progress in improving device architectures and compositional engineering, the external quantum efficiencies (EQE) of the perovskite NC-based LEDs have exceeded 8%.[6,7] However, there is still a room for improvement of these devices as compared with LEDs utilizing traditional II–VI semiconductor quantum dots, where best EQE values currently reach 20%.[8,9]

Recently, metal ion doping has been applied as a tool to tune optical and electronic properties of lead halide perovskite materials.[10] A variety of dopant ions such as $Mn^{2+}$, $Zn^{2+}$, $Cd^{2+}$, $Sn^{2+}$, $Bi^{3+}$, and lanthanide ions have been shown to improve the stability and PL QY of perovskites, tune their Fermi level, and eventually change conductivity characteristics from n-type to p-type.[11–15] Several studies also reported improvements of EQEs of $CsPbBr_3$ NC-based LEDs utilizing the suitable metal ion doping: namely from 0.8% to 1.4% via $Mn^{2+}$ doping;[16] from 1.0% to 4.1% via $Sn^{4+}$ doping;[17] and from 1.6% to 4.4% via $Ce^{3+}$ doping.[18]

In this work, we have utilized the Ag cathode to reduce the electron injection barrier in the $CsPbI_3$ perovskite NC-based LEDs, as compared with similar devices utilizing traditional ITO cathode. More importantly, spontaneous doping of $Ag^+$ ions into the light-emitting layer of $CsPbI_3$ perovskite NCs has been realized, as confirmed by the elemental mapping, X-ray photoelectron spectroscopy (XPS), and the X-ray diffraction (XRD) studies. When the the ITO cathode was replaced with Ag, the peak EQE of $CsPbI_3$ NC-based LEDs was enhanced from 7.3 to 11.2% and the stability of nonencapsulated devices in nitrogen and ambient atmosphere was improved. We discuss in detail beneficial effects of Ag doping and $Ag^+$ ion surface defect passivation on the PL QY and stability of $CsPbI_3$ NCs and LED performance characteristics of the respective devices below.

Figure 1a shows the optical absorption and PL spectra of $CsPbI_3$ NCs in toluene. The absorption and PL peaks are located at 677 and 690 nm, respectively. The NC solution exhibits bright red emission (PL QY over 60%) under 365 nm excitation, with a high color purity [full width at half-maximum (fwhm) equals 36 nm]. The XRD pattern of a $CsPbI_3$ NC

film on a quartz substrate (Figure 1b) matches the reference pattern of the bulk cubic $CsPbI_3$. A transmission electron microscopy (TEM) image of $CsPbI_3$ NCs is given in the inset of Figure 1b and shows the presence of rather monodisperse cubic-shaped NCs with an edge length of 10–12 nm.

Two kinds of multilayer LEDs have been fabricated and compared in this work; the LEDs comprised a patterned ITO or Ag cathode, ZnO NC/polyethylenimine (PEI) bilayer as the electron-transporting layer (ETL), $CsPbI_3$ NC film as the emitting layer, 4,4,4″-tris(carbazol-9-yl)triphenylamine (TCTA) film as the hole-transporting layer (HTL), and $MoO_3$/Au or $MoO_3$/Au/$MoO_3$ as the anode, as presented in Figure 2a. The energy level diagram for all functional layers of these devices is given in Figure 2b. The wide bandgap ZnO NC film was chosen as ETL and at the same time served as a holeblocking layer (HBL) because of its high electron mobility, excellent optical transparency, and the deep-lying VBM (valence band maximum, −7.2 eV).[19] The TCTA film was chosen as HTL and at the same time served as an electron-blocking layer (EBL) because of its suitable highest occupied molecular orbital (HOMO, −5.7 eV) and low electron affinity (−2.3 eV).[20] The combination of ZnO HBL and TCTA EBL sandwiched around the $CsPbI_3$ NC emitting layer allowed for confinement of injected charge carriers resulting in an efficient radiative recombination. The PEI interlayer not only lowered the work function of cathode contacts but also helped to maintain charge neutrality of $CsPbI_3$ NC emitters and preserve their superior emissive properties.[19]

Efficient LEDs require electrodes with both high transparency and low resistance. Metal films are highly conductive but inherently opaque to visible light; therefore, when using them as transparent electrodes, the layer thickness should be low (typically less than 20 nm) to ensure transparency.[21] Metal oxide/metal/metal oxide trilayer structures, on the other hand, are widely employed in LEDs for achieving both high transparency and low resistance.[22] We thus tested different configurations of the cathode and anode trilayers to ensure the fulfillment of the above-mentioned conditions. Because our goal was to replace ITO with Ag, we first attempted to deposit a ZnO-1/Ag/ZnO-2 trilayer structure on the substrate. However, in order to ensure the charge transporting balance, the thickness of the top ZnO-2 film must be at least 40 nm, which hardly provides high transparency. Moreover, as ZnO NC films were deposited from solution, it was difficult to ensure a homogeneous surface morphology and proper grain connectivity if keeping the ZnO-1 layer ultrathin (around 10 nm). For these two reasons, instead of producing LEDs with a transparent cathode, we decided to optimize the anode side to make it transparent, using a $MoO_3$-1/Au/$MoO_3$-2 (MAM) trilayer structure. The $MoO_3$-1 layer was situated between the TCTA and the Au film and served as the hole injection layer. When device parameters of the ITO-based $CsPbI_3$ NC LEDs were systematically checked, an optimum thickness of 20 nm for the $MoO_3$-1 layer was determined for the best-performing devices. A thin 10 nm Au layer was employed to ensure high transparency and at the same time good conductivity of the MAM structure. The $MoO_3$-2 layer was deposited on top of the Au layer to reduce the light reflection at the Au/air interface.[22] Figure 2c shows the two-dimensional optical transmission map of MAM layers with different $MoO_3$-2 thicknesses, indicating that the transmittance reached the highest value for the $MoO_3$-2 layer thickness of 25 nm. As shown in Figure 2d an enhancement in transmission ($\Delta T = T_{25nm} - T_{0nm}$) of about 10% was

achieved in the spectral range of 450–750 nm. In particular, the transmittance of the MAM structure at 690 nm, which is the peak position of the $CsPbI_3$ electroluminescence (EL), increased from 57% to 67% with the 25 nm $MoO_3$-2 film. By employing the four-point probe method, we measured the resistance of the optimized MAM structure to be 15 $\Omega$ $sq^{-1}$, which is thus suitable to serve as an LED anode.

The average peak EQE of the multilayer LEDs increased from 7.3 to 11.2% upon replacing the ITO cathode with Ag (Figure 2e). The insets in Figure 2e show photographs of working devices with Ag and ITO cathodes. The reproducibility of the EQEs of the devices with Ag cathode was high: as shown in Figure S1, an average peak EQE of 11.2% from 26 devices was achieved. Two best-performing devices exhibited an EQE of 12.1%, which is to the best of our knowledge the highest efficiency in $CsPbI_3$ perovskite NC-based LEDs. Voltage-dependent variations of current density and luminance for the devices employing ITO and Ag cathodes are shown in Figure 2f. Even though the ITO film has much higher transmittance (95%) at the EL peak position than the MAM trilayer (67%), as shown in the inset of Figure 2d we found the peak brightness of LEDs with Ag cathode (1106 cd $m^{-2}$) to be more than double that of the ITO-based device (455 cd $m^{-2}$), and the current density of the Ag-based device was lower than that of the ITO-based device under the same voltage, which demonstrates that higher charge injection efficiency was achieved benefiting from the reduction of the electron injection barrier.

For the purpose of identifying the chemical states of constituting elements in the $CsPbI_3$ NC layer (eventually doped with Ag), X-ray photoelectron spectroscopy (XPS) spectra were taken from Ag/ETL/$CsPbI_3$ and ITO/ETL/$CsPbI_3$ films. Panels a, b, and c of Figure 3 show XPS spectra for Pb, I, and Ag elements, respectively, all calibrated with C 1s. No peak shift was observed for Cs 3d (Figure S2), while Pb 4f and I 3d peaks shifted to higher binding energy in Ag/ETL/$CsPbI_3$ as compared to ITO/ETL/$CsPbI_3$ films: for Pb 4f (Figure 3a), the peak shifted from 143.6 to 143.8 eV, and for I 3d (Figure 4b), it shifted from 631.1 to 632.2 eV. These shifts evidence the changes in chemical bonding between the lead cation and iodide anion in $CsPbI_3$,[23] which are associated with the influence of the bottom electrodes (Ag vs ITO). Moreover, as shown in Figure 3c, the Ag 3d peaks appeared for the Ag/ETL/$CsPbI_3$ sample, while no In 3d peaks ($In_2O_3$:$SnO_2$ $\approx$ 9:1 in ITO) have been detected in the ITO/ETL/$CsPbI_3$ sample. Ag 3d spectra consist of two peaks at 374.1 eV ($3d_{3/2}$) and 368.1 eV ($3d_{5/2}$), which can be further deconvoluted into subpeaks at 374.1 and 373.3 eV, and 368.1 and 367.6 eV, corresponding to $3d_{3/2}$ and $3d_{5/2}$ binding energies, respectively. The peaks located at 374.1 and 368.1 eV can be assigned to metal $Ag^0$, while the 373.3 and 367.6 eV peaks are assigned to $Ag^+$.[24]

The presence of Ag 3d peaks in the XPS spectra indicates that silver ions diffused from the underlying Ag electrode into the $CsPbI_3$ NC film. When the Ag-based LED was fabricated, a 100 nm Ag film was first deposited onto the substrate via thermal evaporation, followed by the ZnO film deposition in air and annealing at 120 °C for 10 min. Such a treatment in air may lead to formation of a thin oxide layer of $Ag_2O$ between the Ag cathode and the ZnO film, which serves as a source of $Ag^+$ ions diffusing into the perovskite $CsPbI_3$ film.[25] Upon silver ion diffusion, some may form AgI through reaction with $I^-$ ions at the $CsPbI_3$ NC surface,[26] while others may enter the crystalline lattice of the perovskite. As AgI can readily

decompose into $Ag^0$ under illumination,[27–29] it may produce some metallic Ag on the $CsPbI_3$ NC surface.

The shifts of the peak positions for Pb 4f and I 3d to higher binding energy in the Ag/ETL/$CsPbI_3$ samples (Figure 3a,b) and the presence of $Ag^+$ 3d peaks (Figure 3c) demonstrate that silver ions have become inserted into the crystal structure of the perovskite. This is further supported by the shift of the peak positions in the XRD patterns, shown in Figure 3d. For Ag/ETL/$CsPbI_3$ films, $Ag^+$ ions entered the crystal lattice, as exemplified by the shifts of all XRD peaks to higher angles as compared with ITO/ETL/$CsPbI_3$.[30] This happens because of the shrinkage of the $CsPbI_3$ lattice volume upon the insertion of some $Ag^+$ ions (ionic radius 1.26 Å) taking place of $Cs^+$ (ionic radius 1.67 Å).[31]

To further confirm that the diffusion of silver ions into the perovskite NC film does take place, $CsPbI_3$ NCs from the Ag/ETL/$CsPbI_3$ NC film were redissolved into toluene to carry out TEM, elemental mapping, and energy-dispersive X-ray (EDX) elemental analysis. As shown in Figure S3a, the redissolved NCs mostly maintain the cubic morphology characteristic to $CsPbI_3$ nanoparticles. From the elemental mapping (Figure S3b–f), it can be seen that the Ag element coexists with the Cs, Pb, and I elements from the original perovskite NCs, and all the elements are rather equally distributed. The Ag content was estimated to be 6% from the EDX data. Furthermore, the cross-sectional scanning electron microscopy (SEM) images combined with elemental mapping were collected from the Ag/ETL/$CsPbI_3$ NC film and provided direct evidence for the diffusion of silver ions into the $CsPbI_3$ NCs. As shown in Figure S4, while Cs, Pb, and I ions are almost uniformly distributed over the film profile, the silver content gradually decreases over the distance away from the Ag electrode.

The PL stability of drop-casted $CsPbI_3$ NC films stored at the ambient conditions was compared (Figure 4a). The PL QY of ITO/$CsPbI_3$ samples decreased to ~50% of their initial value within 24 h, while the PL QY of Ag/ETL/$CsPbI_3$ samples maintained 80% of their initial value after 48 h. Note that for the ITO-based samples, the $CsPbI_3$ film stability was enhanced after introducing an ETL (ZnO/PEI), which is due to the PEI passivation of the perovskite NC surface defects.[19] For the Ag-based samples in contrast, the $CsPbI_3$ film stability decreased after introducing an ETL, which is due to the reduced number of $Ag^+$ ions able to diffuse from the underlying Ag substrate. The improved stability of the $CsPbI_3$ NC film may originate from the existence of Ag and/or AgI absorbed on the surface of $CsPbI_3$ NCs, which partially stabilize perovskite NCs from moisture and light irradiation.[32–34] To confirm this hypothesis, we dissolved the $CsPbI_3$ NCs out of Ag/ETL/$CsPbI_3$ films using toluene and collected their TEM images. It was found that most of the $CsPbI_3$ perovskite NCs are covered with dark nanoparticles, as shown in Figure S5a. The elemental mapping characterization (Figure S5b–f) has shown that the dark round particles are either Ag or AgI, which indicates that the diffused silver ions are anchored on the perovskite NC surface in the Ag/ETL/$CsPbI_3$ films in the form of Ag and/or AgI.

Benefiting from the enhanced $CsPbI_3$ NC film stability, the EL stability of the respective devices has been also improved.[35–37] As shown in Figure 4b, the EL intensity of ITO-based $CsPbI_3$ LEDs decreased to ~50% of their initial value in 5 days, while the EL intensity of

Ag-based $CsPbI_3$ LEDs maintained 80% of their initial value after 10 days of storage in a glovebox under nitrogen. In addition, the EL stability of both devices under continuous operation at a constant voltage of 2.5 V was tested under ambient conditions and in the air-free glovebox atmosphere. As shown in Figure S6, the Ag-based devices show better operation stability than ITO-based device when tested in both conditions.

In addition to the observed improvements in stability, brightness, and EQE, the Ag-based devices also exhibited stronger PL than ITO-based ones. The absolute PL QYs of ITO/ETL/$CsPbI_3$, Ag/ETL/$CsPbI_3$, and Ag/$CsPbI_3$ were 60%, 70%, and 81%, respectively, while their PL spectral profiles were the same (Figure S7). The PL lifetime of the Ag/ETL/$CsPbI_3$ film was also longer than that of the ITO/ETL/$CsPbI_3$, as shown in Figure 4c. The average PL lifetime of the cathode/ETL/$CsPbI_3$ structure increased from 4.8 to 8.8 ns when ITO was replaced with Ag. Note that when we increased the amount of $Ag^+$ ions which diffused into the perovskite lattice by removing the ETL, the PL decay transformed from biexponential to monoexponential (Figure 4c), indicating the efficient passivation of surface defects of $CsPbI_3$ NCs by $Ag^+$ ions.[38,39] The average PL lifetime of Ag/$CsPbI_3$ samples increased to 15.4 ns. The elongated emission lifetime and improved PL QY of Ag/ETL/$CsPbI_3$ NC films ensure the higher brightness and EQE compared with that of ITO/ETL/$CsPbI_3$-based devices.

In order to further confirm the beneficial effect of silver on $CsPbI_3$ NCs, the following control experiment was performed. As shown in Figure S8, we added $AgC_2H_3O_2$–OLA solution (equivalent volume with different $Ag^+$ concentration) into $CsPbI_3$ NC solution (equivalent volume with the same concentration). The band tail states in absorption spectra disappeared (Figure S8a) and the PL intensity increased (Figure S8b) when $Ag^+$ ions were introduced, demonstrating the passivation of surface defects of $CsPbI_3$ NCs.[40,41] In addition, all $CsPbI_3$ NCs treated with silver ions exhibited improved stability, as shown in Figure S8c,. These results provide additional evidence that silver ions play an important role in improving optical characteristics of $CsPbI_3$ NCs, thus enhancing the LED performance.

Both hole and electron transport properties of multilayer LEDs were enhanced, as seen from comparison of the respective “electron-only” and “hole-only” devices. For the electron-only devices, a structure of (ITO or Ag)/ZnO/$CsPbI_3$ NC/LiF/Al was employed. For the hole-only devices, a structure of (ITO or Ag)/PEDOT:PSS/$CsPbI_3$ NC/TCTA/$MoO_3$/Au was employed. As shown in Figure 4d, the currents of all Ag-based devices were higher than that of ITO-based devices.

In conclusion, we have developed a method of simultaneous doping and surface passivation of $CsPbI_3$ NC films with silver. Some $Ag^+$ ions substitute $Cs^+$ ions in the lattice structure of perovskites, which leads to their stabilization; passivation of $CsPbI_3$ NC surface with $Ag^+$ ions converts nonradiative trap states to radiative states, resulting in the enhancement of PL QY. In the LEDs utilizing Ag-doped $CsPbI_3$ NCs as emitting layer, Ag was chosen as a cathode to reduce the electron injection barrier, and trilayer $MoO_3$/Au/$MoO_3$ structure served as an anode to ensure the high transparency and good conductivity. As a result, the charge carrier transport properties of $CsPbI_3$ films have been improved, which led to

cumulative enhancement of the performance of Ag-doped $CsPbI_3$ NC-based LEDs employing the silver cathodes, with EQE averaging 11.2%.

## Supplementary Material

Refer to Web version on PubMed Central for supplementary material.

## ACKNOWLEDGMENTS

We acknowledge financial support from the Natural Science Foundation of China (NSFC) (61675086, 61475062, 61722504, 51702115, 51772123, and 11674127); National Key Research and Development Program of China (2017YFB0403601); Jilin Province Science Fund for Excellent Young Scholars (20170520129JH); China Postdoctoral Science Foundation (2017M611319); National Postdoctoral Program for Innovative Talents (BX201600060); BORSF RCS; Institutional Development Award (P20GM103424); the Research Grant Council of Hong Kong S.A.R. (GRF project CityU11337616 and NSFC/RGC Joint Research Scheme project N_CityU108/17); and the Open Research Fund of State Key Laboratory of Polymer Physics and Chemistry, Changchun Institute of Applied Chemistry, Chinese Academy of Sciences.

## REFERENCES

(1). Protesescu L; Yakunin S; Bodnarchuk MI; Krieg F; Caputo R; Hendon CH; Yang RX; Walsh A; Kovalenko MV Nanocrystals of Cesium Lead Halide Perovskites ($CsPbX_3$, X = Cl, Br, and I): Novel Optoelectronic Materials Showing Bright Emission with Wide Color Gamut. Nano Lett. 2015, 15, 3692–3696. [PubMed: 25633588]

(2). Li X; Wu Y; Zhang S; Cai B; Gu Y; Song J; Zeng H Quantum Dots: $CsPbX_3$ Quantum Dots for Lighting and Displays: Room-Temperature Synthesis, Photoluminescence Superiorities, Underlying Origins and White Light-Emitting Diodes. Adv. Funct. Mater 2016, 26, 2435–2445.

(3). Hu F; Yin C; Zhang H; Sun C; Yu WW; Zhang C; Wang X; Zhang Y; Xiao M Slow Auger Recombination of Charged Excitons in Nonblinking Perovskite Nanocrystals without Spectral Diffusion. Nano Lett. 2016, 16, 6425–6430.

(4). Huang H; Polavarapu L; Sichert JA; Susha AS; Urban AS ; Rogach AL Colloidal Lead Halide Perovskite Nanocrystals: Synthesis, Optical Properties and Applications. NPG Asia Mater. 2016, 8, e328.

(5). Yin C; Chen L; Song N; Lv Y; Hu F; Sun C; Yu WW; Zhang C; Wang X; Zhang Y; et al. Bright-Exciton Fine-Structure Splittings in Single Perovskite Nanocrystals. Phys. Rev. Lett 2017, 119, 026401. [PubMed: 28753331]

(6). Chiba T; Hoshi K; Pu YJ; Takeda Y; Hayashi Y; Ohisa S; Kawata S; Kido J High Efficiency Perovskite Quantum-Dot Light-Emitting Devices by Effective Washing Process and Interfacial Energy Level Alignment. ACS Appl. Mater. Interfaces 2017, 9, 18054–18060. [PubMed: 28485139]

(7). Yan F; Xing J; Xing G; Quan L; Tan ST; Zhao J; Su R; Zhang L; Chen S; Zhao Y; et al. Highly Efficient Visible Colloidal Lead-Halide Perovskite Nanocrystal Light-Emitting Diodes. Nano Lett. 2018, 18, 3157–3164. [PubMed: 29608317]

(8). Dai X; Zhang Z; Jin Y; Niu Y; Cao H; Liang X; Chen L; Wang J; Peng X Solution-Processed, High-Performance Light-Emitting Diodes Based on Quantum Dots. Nature 2014, 515, 96–99. [PubMed: 25363773]

(9). Zhang H; Sun X; Chen S Light-Emitting Diodes: Over 100 cd $A^{-1}$ Efficient Quantum Dot Light-Emitting Diodes with Inverted Tandem Structure. Adv. Funct. Mater 2017, 27, 1700610.

(10). Swarnkar A; Ravi VK; Nag A Beyond Colloidal Cesium Lead Halide Perovskite Nanocrystals: Analogous Metal Halides and Doping. ACS Energy Lett. 2017, 2, 1089–1098.

(11). Begum R; Parida MR; Abdelhady AL; Murali B; Alyami NM; Ahmed GH; Hedhili MN; Bakr OM; Mohammed OF Engineering Interfacial Charge Transfer in $CsPbBr_3$ Perovskite Nanocrystals by Heterovalent Doping. J. Am. Chem. Soc 2017, 139, 731–737. [PubMed: 27977176]

(12). van der Stam W; Geuchies JJ; Altantzis T; van den Bos KHW; Meeldijk JD; Van Aert S; Bals S; Vanmaekelbergh D; de Mello Donega C Highly Emissive Divalent-Ion-Doped Colloidal $CsPb_{1-x}M_xBr_3$ Perovskite Nanocrystals through Cation Exchange. J. Am. Chem. Soc 2017, 139, 4087–4097. [PubMed: 28260380]

(13). Liu W; Lin Q; Li H; Wu K; Robel I; Pietryga JM; Klimov VI $Mn^{2+}$-Doped Lead Halide Perovskite Nanocrystals with Dual-Color Emission Controlled by Halide Content. J. Am. Chem. Soc 2016, 138, 14954–14961. [PubMed: 27756131]

(14). Pan G; Bai X; Yang D; Chen X; Jing P; Qu S; Zhang L; Zhou D; Zhu J; Xu W; et al. Doping Lanthanide into Perovskite Nanocrystals: Highly Improved and Expanded Optical Properties. Nano Lett. 2017, 17, 8005–8011. [PubMed: 29182877]

(15). Zhu J; Yang X; Zhu Y; Wang Y; Cai J; Shen J; Sun L; Li C Room-Temperature Synthesis of Mn-Doped Cesium Lead Halide Quantum Dots with High Mn Substitution Ratio. J. Phys. Chem. Lett 2017, 8, 4167–4171. [PubMed: 28819974]

(16). Zou S; Liu Y; Li J; Liu C; Feng R; Jiang F; Li Y; Song J; Zeng H; Hong M; et al. Stabilizing Cesium Lead Halide Perovskite Lattice through Mn (II)-Substitution for Air-Stable Light-Emitting Diodes. J. Am. Chem. Soc 2017, 139, 11443–11450. [PubMed: 28756676]

(17). Wang HC; Wang W; Tang AC; Tsai HY; Bao Z; Ihara T; Yarita N; Tahara H; Kanemitsu Y; Chen S High-Performance Novel $CsPb_{1-x}Sn_xBr_3$ Perovskite Quantum Dots for Highly-Efficient Light-Emitting Diodes. Angew. Chem. Int. Ed 2017, 56, 13650–13654.

(18). Yao J; Ge J; Han BN; Wang KH; Yao HB; Yu HL; Li JH; Zhu BS; Song J; Chen C; et al. $Ce^{3+}$-Doping to Modulate Photoluminescence Kinetics for Efficient $CsPbBr_3$ Nanocrystals Based Light-Emitting Diodes. J. Am. Chem. Soc 2018, 140, 3626–3634. [PubMed: 29341604]

(19). Zhang X; Sun C; Zhang Y; Wu H; Ji C; Chuai Y; Wang P; Wen S; Zhang C; Yu WW Bright Perovskite Nanocrystal Films for Efficient Light-Emitting Devices. J. Phys. Chem. Lett 2016, 7, 4602–4610. [PubMed: 27758105]

(20). Wang J; Wang N; Jin Y; Si J; Tan Z-K; Du H; Cheng L; Dai X; Bai S; He H; et al. Interfacial Control Toward Efficient and Low-Voltage Perovskite Light-Emitting Diodes. Adv. Mater 2015, 27, 2311–2316. [PubMed: 25708283]

(21). Yambem SD; Ullah M; Tandy K; Burn PL; Namdas EB ITO-Free Top Emitting Organic Light Emitting Diodes with Enhanced Light Out-Coupling. Laser Photonics Rev. 2014, 8, 165–171.

(22). Wu H; Zhang Y; Zhang X; Lu M; Sun C; Bai X; Zhang T; Sun G; Yu WW Fine-Tuned Multilayered Transparent Electrode for Highly Transparent Perovskite Light-Emitting Devices. Adv. Electron. Mater 2018, 4, 1700285.

(23). Nam JK; Chai SU; Cha W; Choi YJ; Kim W; Jung MS; Kwon J; Kim D; Park JH Potassium Incorporation for Enhanced Performance and Stability of Fully Inorganic Cesium Lead Halide Perovskite Solar Cells. Nano Lett. 2017, 17, 2028–2033. [PubMed: 28170276]

(24). Lee S; Park JH; Bo RL; Jung ED; Yu JC; Nuzzo DD; Friend RH; Song MH Amine-Based Passivating Materials for Enhanced Optical Properties and Performance of Organic-Inorganic Perovskite in Light-Emitting Diodes. J. Phys. Chem. Lett 2017, 8, 1784–1792. [PubMed: 28378585]

(25). Chen CW; Hsieh PY; Chiang HH; Lin CL; Wu HM; Wu CC Top-Emitting Organic Light-Emitting Devices Using Surface-Modified Ag Anode. Appl. Phys. Lett 2003, 83, 5127–5129.

(26). Back H; Kim G; Kim J; Kong J; Kim TK; Kang H; Kim H; Lee J; Lee S; Lee K Achieving Long-Term Stable Perovskite Solar Cells via Ion Neutralization. Energy Environ. Sci 2016, 9, 1258–1263.

(27). Lin H; Cao J; Luo B; Xu B; Chen S Synthesis Of Novel Z-Scheme AgI/Ag/AgBr Composite with Enhanced Visible Light Photocatalytic Activity. Catal. Commun 2012, 21, 91–95.

(28). Zheng Z; Chen C; Bo A; Zavahir FS; Waclawik ER; Zhao J; Yang D; Zhu H Visible-Light-Induced Selective Photocatalytic Oxidation of Benzylamine into Imine over Supported Ag/AgI Photocatalysts. ChemCatChem 2014, 6, 1210–1214.

(29). Yu C; Wei L; Zhou W; Chen J; Fan Q; Liu H Enhancement of the Visible Light Activity and Stability of $Ag_2CO_3$ by Formation of $AgI/Ag_2CO_3$ Heterojunction. Appl. Surf. Sci 2014, 319, 312–318.

(30). Akkerman QA; Meggiolaro D; Dang Z; De Angelis F; Manna L Fluorescent Alloy $CsPb_xMn_{1-x}I_3$ Perovskite Nanocrystals with High Structural and Optical Stability. ACS Energy Lett. 2017, 2, 2183–2186. [PubMed: 29142911]

(31). Swarnkar A; Mir WJ; Nag A Can B-Site Doping or Alloying Improve Thermal- and Phase-Stability of All-Inorganic $CsPbX_3$ (X = Cl, Br, I) Perovskites? ACS Energy Lett. 2018, 3, 286–289.

(32). Luo B; Pu YC; Lindley SA; Yang Y; Lu L; Li Y; Li X; Zhang JZ Organolead Halide Perovskite Nanocrystals: Branched Capping Ligands Control Crystal Size and Stability. Angew. Chem 2016, 128, 9010–9014.

(33). Yang D; Li X; Zeng H Surface Chemistry of All Inorganic Halide Perovskite Nanocrystals: Passivation Mechanism and Stability. Adv. Mater. Interfaces 2018, 5, 1701662.

(34). Krieg F; Ochsenbein ST; Yakunin S; ten Brinck S; Aellen P; Süess A; Clerc B; Guggisberg D; Nazarenko O; Shynkarenko Y; et al. Colloidal $CsPbX_3$ (X = Cl, Br, I) Nanocrystals 2.0: Zwitterionic Capping Ligands for Improved Durability and Stability. ACS Energy Lett. 2018, 3, 641–646. [PubMed: 29552638]

(35). Swarnkar A; Marshall AR; Sanehira EM; Chernomordik BD; Moore DT; Christians JA; Chakrabarti T; Luther JM Quantum Dot-Induced Phase Stabilization of A-$CsPbI_3$ Perovskite for High-Efficiency Photovoltaics. Science 2016, 354, 92–95. [PubMed: 27846497]

(36). Zou C; Huang CY; Sanehira EM; Luther J; Lin LY Highly Stable Cesium Lead Iodide Perovskite Quantum Dot Light-Emitting Diodes. Nanotechnology 2017, 28, 455201. [PubMed: 29039355]

(37). Sim KM; Swarnkar A; Nag A; Chung DS Phase Stabilized α-CsPbI3 Perovskite Nanocrystals for Photodiode Applications. Laser Photonics Rev. 2018, 12, 1700209.

(38). Zhou J; Zhu M; Meng R; Qin H; Peng X Ideal CdSe/CdS Core/Shell Nanocrystals Enabled by Entropic Ligands and Their Core Size-, Shell Thickness-, and Ligand-Dependent Photoluminescence Properties. J. Am. Chem. Soc 2017, 139, 16556–16567. [PubMed: 29094943]

(39). Koscher BA; Swabeck JK; Bronstein ND; Alivisatos AP Essentially Trap-Free $CsPbBr_3$ Colloidal Nanocrystals by Postsynthetic Thiocyanate Surface Treatment. J. Am. Chem. Soc 2017, 139, 6566–6569. [PubMed: 28448140]

(40). Liu M; Voznyy O; Sabatini R; Arquer FPGD; Munir R; Balawi AH; Lan X; Fan F; Walters G; Kirmani AR; et al. Hybrid Organic-Inorganic Inks Flatten the Energy Landscape in Colloidal Quantum Dot Solids. Nat. Mater 2017, 16, 258. [PubMed: 27842072]

(41). Woo JY; Kim Y; Bae J; Kim TG; Kim JW; Lee DC; Jeong S Highly Stable Cesium Lead Halide Perovskite Nanocrystals through in Situ Lead Halide Inorganic Passivation. Chem. Mater 2017, 29, 7088–7092.

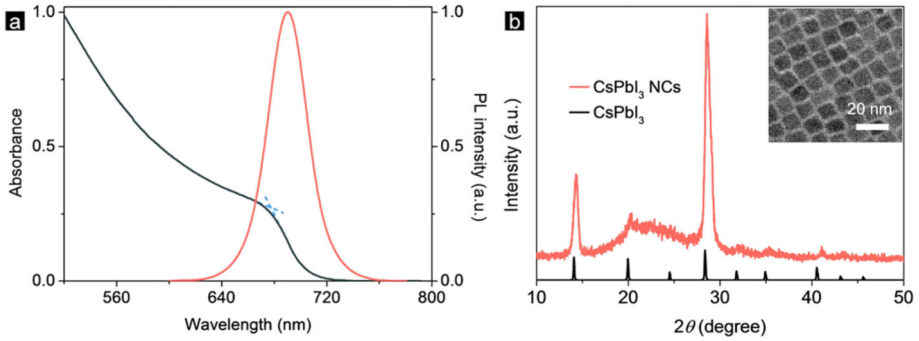


**Figure 1.**

(a) Absorption (black) and PL (red) spectra of $CsPbI_3$ NCs in toluene. (b) XRD pattern of the $CsPbI_3$ NC film on quartz substrate (red); reference pattern for bulk $CsPbI_3$ is provided in black. Inset in panel b shows the TEM image of $CsPbI_3$ NCs.

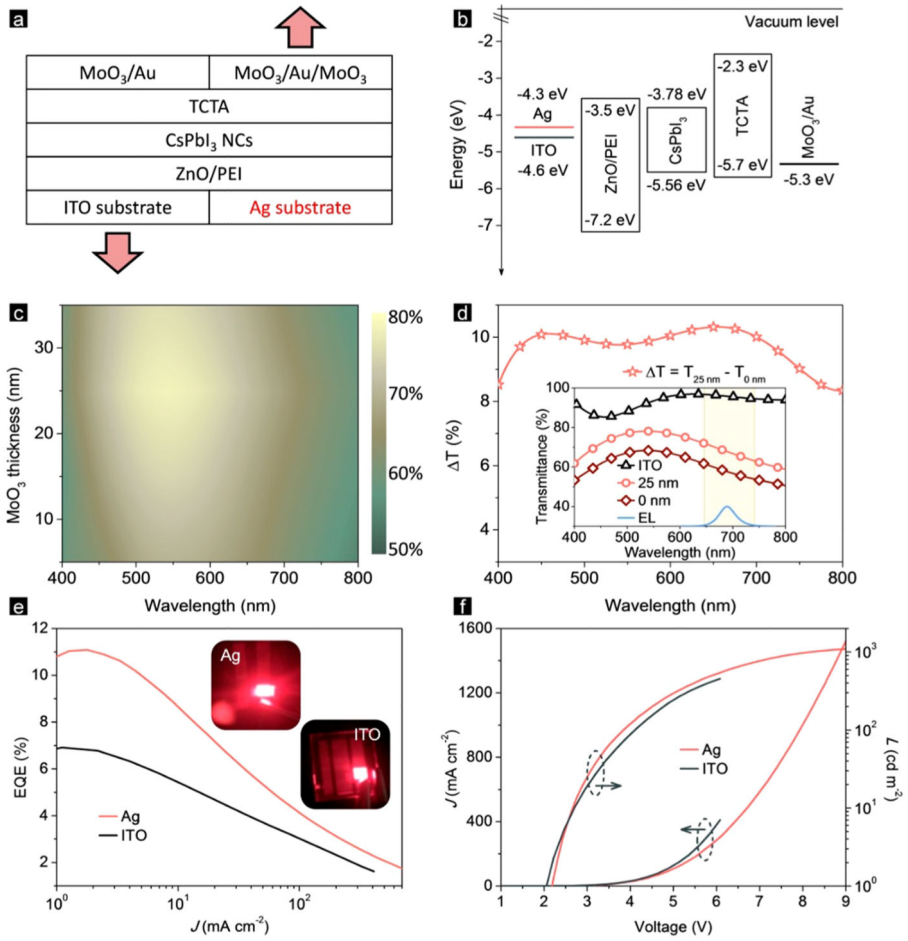


**Figure 2.**

(a) Schematic diagrams of the $CsPbI_3$ NC-based LEDs with ITO and Ag bottom cathodes. Red arrows indicate on which side the respective devices are transparent and emit light. (b) Energy level diagram for all functional layers mentioned in panel a. (c) Color map of the optical transmission of MAM structure with different $MoO_3$-2 layer thickness. (d) Transmission enhancement of MAM structure with a 25 nm $MoO_3$-2 layer. Inset in panel d shows transmittance for ITO, $M_{20}AM_0$, and $M_{20}AM_{25}$ layers and an EL spectrum of LED. (e) EQE vs current density for LEDs with Ag and ITO cathodes; insets show photographs of the respective working devices. (f) Current density vs driving voltage and luminance vs driving voltage for LEDs with Ag and ITO cathodes.

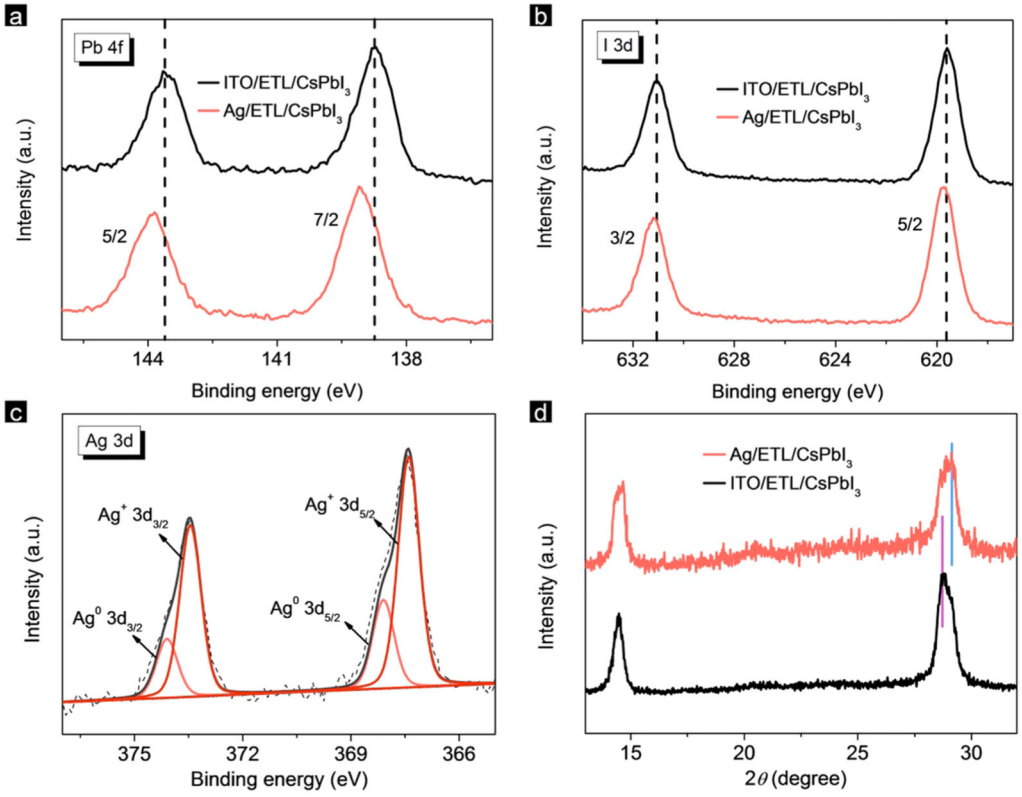


**Figure 3.**

XPS spectra of ITO/ETL/$CsPbI_3$ (black) and Ag/ETL/$CsPbI_3$ (red) films for (a) Pb 4f, (b) I 3d, and (c) Ag 3d elements. (d) XRD patterns for Ag/ETL/$CsPbI_3$ (red) and ITO/ETL/$CsPbI_3$ (black) films.

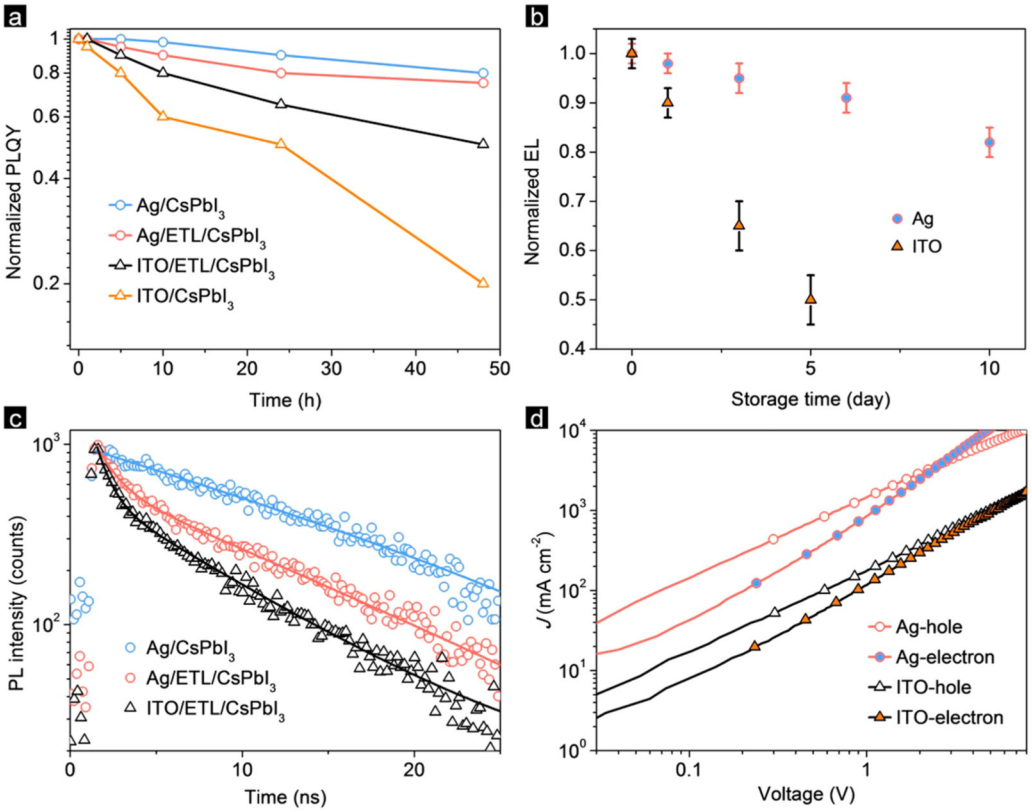


**Figure 4.**

(a) Changes of PL QYs (normalized for the initial point) of $CsPbI_3$ NC films on different substrates (as indicated in the panel) stored in air for 2 days. (b) Changes of EL intensity of $CsPbI_3$ NC-based LEDs with ITO and Ag bottom layers, in nitrogen atmosphere. (c) PL decays of $Ag/CsPbI_3$, $Ag/ETL/CsPbI_3$, and $ITO/ETL/CsPbI_3$ films. (d) Current density vs voltage curves of the “electron-only” and “hole-only” LEDs, with the respective structures as indicated in the panel.